

## Direct Determination of Sizes of Excitations from Optical Measurements on Ion-Implanted GaAs

D. E. Aspnes

*Bell Laboratories, Murray Hill, New Jersey 07974*

and

S. M. Kelso

*Xerox Palo Alto Research Center, Palo Alto, California 94304*

and

C. G. Olson and D. W. Lynch

*Ames Laboratory and Department of Physics, Iowa State University, Ames, Iowa 50011*

(Received 25 March 1982)

Using a simple model that describes the decrease of the amplitudes of optical structures in ion-implanted crystals, projected areas of several valence and core excitons in GaAs are determined. The last remnant of crystal-related optical structure vanishes for crystallite areas less than  $(16 \text{ \AA})^2$ .

PACS numbers: 71.25.-s, 71.35.+z, 78.20.Dj, 78.40.Fy

As is well known, an energetic ion traveling in a nonchanneling direction leaves a trail of defects and dislocations in an otherwise perfect crystal.<sup>1</sup> The disruption of periodicity and the breakdown of selection rules in the damaged material lead to a number of effects in all regions of the optical spectrum, including increased absorption near the fundamental edge,<sup>2</sup> destruction of sharp features,<sup>3-5</sup> and the quenching of luminescence lines due to sharply decreased excitation lifetimes, a result of enhanced recombination probability at defect sites.<sup>6</sup> At sufficiently high fluences, the damage tracks overlap and the solid becomes indistinguishable from amorphous material prepared in other ways.<sup>7</sup>

In this Letter, we show that the rate at which sharp spectral features disappear with increasing fluence contains information not previously recognized; specifically, the projected areas of the excitations responsible for structures in optical spectra. The analysis requires only the existence of a spectral characteristic, such as a structure in a higher-derivative optical spectrum, that can be related uniquely to a particular type of excitation and that is quenched (broadened beyond detection) if the excitation overlaps a damage track. The connection to excitation size can be established qualitatively as follows. If the radius of the excitation is large compared to that of the damage track, then the probability of overlap, and thus the amount of material rendered inactive by an energetic ion, is a function only of the area of the excitation projected onto the plane perpendicular to the track. If the damage tracks are lo-

cated randomly, then the amount of material rendered inactive by the next ion is proportional to the active fraction still remaining. Under these conditions Poisson statistics apply and the relative decrease in amplitude is simply given by  $\exp(-Fa)$ , where  $F$  is the total fluence and  $a$  is the projected area of the excitation.

Here, we apply this analysis to optical data for several valence- and core-to-conduction band transitions in GaAs. The projected areas obtained for the  $E_1$  and  $E_1 + \Delta_1$  excitonic resonances,  $(100 \text{ \AA})^2$  and  $(90 \text{ \AA})^2$ , respectively, are in good agreement with the theoretical estimate,  $(91 \text{ \AA})^2$ , calculated for  $E_1 + \Delta_1$  from independently determined parameters. The results for other excitonic resonances are  $(82 \text{ \AA})^2$  for  $E_0'$ ,  $(63 \text{ \AA})^2$  for  $E_2$ , and  $(31 \text{ \AA})^2$  for the well-resolved Ga  $3d$  core-level transition to  $L$ . The small radius for the core exciton shows that this excitation is relatively tightly bound, and is consistent with previous evidence<sup>8-10</sup> obtained from binding-energy and  $L$ - $X$  mixing arguments for the existence of a strong central-cell component in the potential energy. At large fluences, the last remnant of structure to vanish in the crystalline spectrum is  $E_2$ , which disappears at a rate characteristic of a projected area of  $(16 \text{ \AA})^2$ . The latter result shows that visible-near-uv optical spectra are as sensitive to amorphicity and polycrystallinity as x-ray,<sup>11</sup> electron,<sup>12</sup> or Raman<sup>13</sup> scattering, or even more so. Moreover, because optical penetration depths in the  $E_2$  region are typically 50–100  $\text{\AA}$ , very little material is needed, so the characterization method is directly applicable to thin films.

To test the model, we studied a series of  $\langle 100 \rangle$  GaAs single crystals implanted  $7^\circ$  off axis to various fluences with 270-keV  $\text{As}^+$  ions. The penetration depth of these ions,  $\sim 1100 \text{ \AA}$ , is effectively infinite in comparison to the penetration depth of light,  $70\text{--}200 \text{ \AA}$ , so that straggling effects can be ignored. In the visible-near-uv spectral range, high-precision dielectric-function data were obtained by spectroscopic ellipsometry using methods described elsewhere.<sup>14</sup> Third joint-density-of-states (3JDOS) derivatives were calculated numerically from these data and are shown in Fig. 1. Two prerequisites for the model's applicability are well satisfied: Sharp structures exist, and these structures initially decrease in amplitude with essentially invariant line shapes as the fluence increases. Note particularly that the three  $E_0'$  structures at 4.47, 4.65, and 4.87 eV decrease as a unit, more rapidly than the  $E_2$  structure at 5.00 eV. At the highest fluence shown, only the  $E_2$  structure remains.

The upper portion of Fig. 2 shows a semilogarithmic plot of the peak-to-peak height of the  $E_0'$  and  $E_2$  structures of Fig. 1 as a function of fluence. Another prerequisite for the applicability of the model is also satisfied: The peak-to-peak heights decrease exponentially with increasing fluence. Consequently, the slopes can be interpreted as projected areas of the excitations. We find from

the straight lines shown projected areas of  $(85 \text{ \AA})^2$  and  $(63 \text{ \AA})^2$  for the  $E_0'$  and  $E_2$  transitions. A similar analysis of data for the  $E_1$  and  $E_1 + \Delta_1$  transitions has also been done and will be presented elsewhere; the projected areas for these transitions are  $(100 \text{ \AA})^2$  and  $(90 \text{ \AA})^2$ .

We next establish the connection between the projected area and more usual size parameters such as excitonic radii. For this purpose we focus on the  $E_1 + \Delta_1$  excitonic resonance, because all parameters necessary to calculate its radius at room temperature have been determined experimentally.<sup>15</sup> The resonance is essentially two-dimensional because of the large longitudinal/transverse interband mass ratio along the  $\langle 111 \rangle$  direction, and its room-temperature transverse reduced mass,  $\mu_t = 0.053m_e$ ,<sup>15</sup> has been deduced from the period of Franz-Keldysh oscillations. Using the static dielectric constant  $\epsilon = 13.5$  for GaAs, we find  $r_{ex} = \hbar^2 \epsilon / (2\mu_t e^2) = 67 \text{ \AA}$ . Projecting the area corresponding to this radius onto the  $\langle 100 \rangle$  surface leads to an effective area of  $(91 \text{ \AA})^2$ , compared to the experimentally determined value of  $(90 \text{ \AA})^2$ . The agreement is somewhat fortuitous since we neglected the finite size of the damage trail. However, it establishes the fact that the projected area determined from ion-implantation

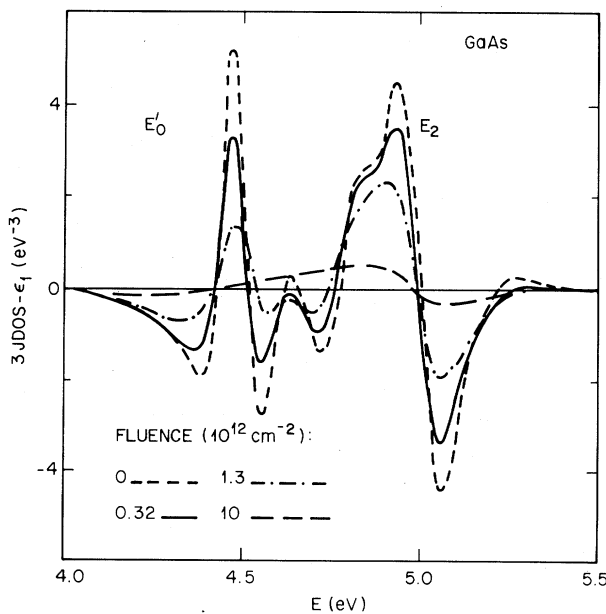


FIG. 1. Third joint-density-of-states derivatives of  $\epsilon_1$  spectra for GaAs crystals selectively damaged with 270-keV  $\text{As}^+$  ions at various fluences.

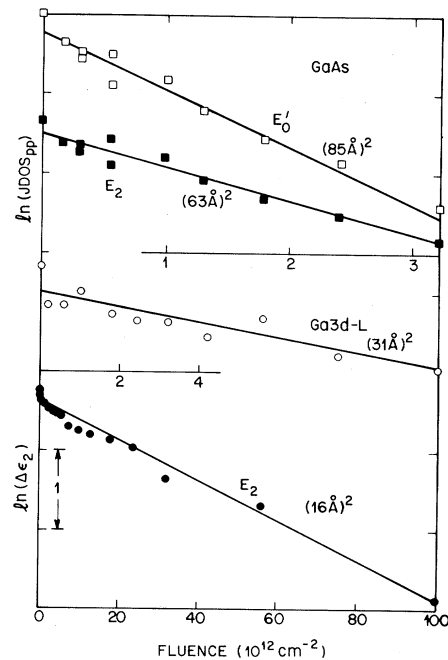


FIG. 2. Semilogarithmic plots of measured peak heights of 3JDOS ( $E_0'$ ,  $E_2$ ), 2EDR (Ga  $3d-L$ ), and dielectric response ( $E_2$ ) structures as a function of fluence.

data is closely related to more conventional measures of excitation sizes.

We now turn to the original motivation of the experiment, which was to measure the sizes of excitations associated with shallow core levels in semiconductors. Despite mounting evidence<sup>8-10</sup> in the form of large binding energies and a strong central-cell component to the potential, the departure from effective-mass-approximation (EMA) behavior is still not clearly understood. We performed a similar analysis for second-energy-derivative reflectance (2EDR) spectra of the well-resolved Ga  $3d-L$  structure at 20.3 eV. The results for peak-to-peak heights versus fluence are shown in the central portion of Fig. 2. The variation is again accurately exponential, and yields a projected area of  $(31 \text{ \AA})^2$ . Assuming for simplicity that  $m_t^* \ll m_l^*$  for the  $L_1^c$  minimum, we calculate a radius  $r_0 = 23 \text{ \AA}$ . This should be compared to the effective-mass estimate of  $47 \text{ \AA}$ , which is evaluated with  $m_t^* = 0.0754m_0$ .<sup>16</sup> Consequently, these new results are consistent with previous work that indicates a non-EMA character for core-level excitations.

A related problem of current interest, particularly in thin-film technology, is to determine minimum grain sizes for which crystalline effects can be positively identified, and consequently for which the material can be considered polycrystalline rather than amorphous. In general, the definition of minimum grain size depends on the response being measured. For example, the minimum grain sizes that can be detected in x-ray, electron, and Raman scattering measurements on semiconductors are of the order of  $10$ ,<sup>11</sup>  $10$ ,<sup>12</sup> and  $20 \text{ \AA}$ ,<sup>13</sup> respectively. However, more relevant for thin-film solar-cell technology is the minimum size determined by the near-ir, visible, and near-uv polarizability. Schwidofsky<sup>17</sup> has reported that the infrared refractive indices increase with decreasing grain size down to  $10 \text{ \AA}$  as determined by reflective electron scattering measurements on deposited Si films, but the infrared data could not provide information on the responsible transitions.

In Fig. 3, we present a series of  $\epsilon_2$  spectra for fluences near the complete transformation to amorphous material. The last crystal-related feature to vanish is  $E_2$ . If we use the  $\epsilon_2$  value of the amorphized material as a base line and plot the difference between peak height and base line in Fig. 3, the variation is also accurately exponential as seen in the lower portion of Fig. 2. In this case, the decrease of amplitude with increas-

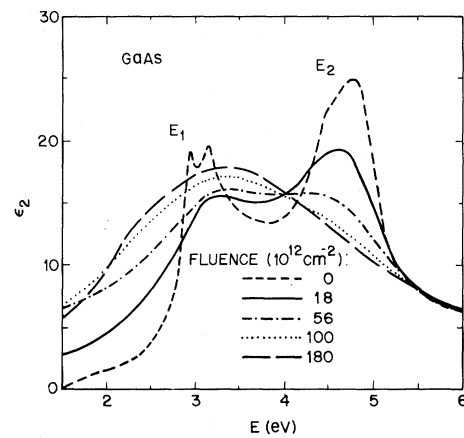


FIG. 3. Disappearance of crystal-related structure in  $\epsilon_2$  spectra with increasing fluence.

ing fluence is interpreted as the decreasing probability of finding a crystallite with the minimum area necessary to produce a recognizable crystalline response. This area is  $(16 \text{ \AA})^2$ .

The equivalent diameter for a circular cross section,  $18 \text{ \AA}$ , is larger than the  $10\text{-\AA}$  limit deduced by Schwidofsky. One possible explanation is that our diameter is larger because we have not taken the finite sizes of the damage tracks into account. The assumption that both grain-size estimates are accurate leads to an effective damage-track diameter over the penetration depth of light of the order of, and certainly no greater than,  $10 \text{ \AA}$ . This small upper limit justifies our previous assumption that the damage-trail radius is not a significant factor in determination of the projected areas of the other transitions. A second possibility is that the mean grain size measured by electron scattering actually is much smaller than the larger grains responsible for the crystalline response measured here. We note that the complete transition to amorphous material occurs for a fluence of about  $1 \times 10^{14} \text{ cm}^{-2}$ , which corresponds to an area per ion of  $(10 \text{ \AA})^2$ .

Our discussion has deliberately been qualitative because the model is simple enough so that its essential features can be described at this level. However, a quantitative treatment of the projected area can easily be formulated by using time-dependent perturbation theory.<sup>18</sup> In general, one finds that the increase in the decay probability of an excitation is proportional to the square of a matrix element involving  $\Delta V(\vec{r} - \vec{R}_\nu)$ , the difference between the unperturbed crystal potential and that with damage track passing through  $\vec{R}_\nu$ . The relevant wave functions are those of the exci-

tation and the states into which it can decay. The qualitative approach given here corresponds approximately to choosing a value of  $\Delta V$  that is large near  $\bar{R}_v$  and zero elsewhere. The exact form of  $\Delta V$  could be determined in principle if the microscopic nature of the damage were known. But if the radius of the excitation is much larger than that of  $\Delta V$ , the details of  $\Delta V$  will not be important. A more extended treatment will be given elsewhere.

We gratefully acknowledge the technical assistance of L. J. Smith, D. E. Post, and M. W. Focht, who performed the ion implantations, and the hospitality of the Synchrotron Radiation Center, University of Wisconsin-Madison, at which the 2EDR measurements were made. The storage ring is operated under National Science Foundation Contract No. DMR 7721888. Ames Laboratory is operated by Iowa State University under U. S. Department of Energy Contract No. W-7405-Eng-82. This part of the work was supported by the Office of Basic Energy Sciences.

<sup>1</sup>K. Winterbon, *Ion Implantation Range and Energy Deposition Distributions* (IFI/Plenum, New York, 1975), Vol. 2.

<sup>2</sup>Q. Kim and Y. S. Park, *J. Appl. Phys.* **51**, 2024 (1980).

<sup>3</sup>V. Grasso, G. Mondio, G. Saitta, S. U. Campisano,

G. Foti, and E. Rimini, *Appl. Phys. Lett.* **33**, 632 (1978).

<sup>4</sup>D. E. Aspnes and A. A. Studna, *Surf. Sci.* **96**, 294 (1980).

<sup>5</sup>J. B. Theeten and M. Erman, *J. Vac. Sci. Technol.* **20**, 471 (1982).

<sup>6</sup>M. Kawabe, N. Kanzaki, K. Masuda, and S. Namba, *Appl. Opt.* **17**, 2556 (1978).

<sup>7</sup>J. Bourgoïn, *Solid State Commun.* **34**, 25 (1980).

<sup>8</sup>D. E. Aspnes, C. G. Olson, and D. W. Lynch, in *Proceedings of the Thirteenth International Conference on the Physics of Semiconductors, Rome*, edited by F. G. Fumi (Tipografia Marves, Rome, 1976), p. 1000.

<sup>9</sup>S. M. Kelso, D. E. Aspnes, C. G. Olson, D. W. Lynch, and D. Finn, *Phys. Rev. Lett.* **45**, 1032 (1980).

<sup>10</sup>D. E. Aspnes, S. M. Kelso, C. G. Olson, D. W. Lynch, and D. Finn, *J. Phys. Soc. Jpn.* **49**, Suppl. A, 109 (1980).

<sup>11</sup>See, e.g., H. P. Klug and L. E. Alexander, *X-Ray Diffraction Procedures* (Wiley, New York, 1974), 2nd ed., Chap. 9.

<sup>12</sup>G. Schimmel, *Elektronenmikroskopische Methodik* (Springer, Berlin, 1969), p. 45.

<sup>13</sup>R. Tsu, S. S. Chao, S. R. Ovshinsky, G. Jan, and F. H. Pollak, *J. Phys. Paris, Colloq.* **41**, C4-269 (1981).

<sup>14</sup>D. E. Aspnes and A. A. Studna, *Appl. Opt.* **14**, 220 (1975), and *Rev. Sci. Instrum.* **49**, 291 (1978), and *Appl. Phys. Lett.* **39**, 316 (1981).

<sup>15</sup>S. Pond and P. Handler, *Phys. Rev. B* **8**, 2869 (1973).

<sup>16</sup>D. E. Aspnes, *Phys. Rev. B* **14**, 5331 (1976).

<sup>17</sup>F. Schwidefsky, *Thin Solid Films* **18**, 45 (1973).

<sup>18</sup>L. I. Schiff, *Quantum Mechanics* (McGraw-Hill, New York, 1955), 2nd ed.